Optics Letters

Mid-infrared wavelength conversion from As_2Se_3 microwires

Lizhu Li,* Nurmemet Abdukerim, and Martin Rochette

Department of Electrical and Computer Engineering, 3480 University Street, McGill University, Montreal H3A 2A7, Canada
**Corresponding author: lizhu.li@mail.mcgill.ca*

Received 17 November 2016; revised 17 December 2016; accepted 2 January 2017; posted 5 January 2017 (Doc. ID 280730); published 1 February 2017

We demonstrate all-fiber far-detuned and widely tunable mid-infrared wavelength conversion using As_2Se_3 microwires. In a first experiment, an idler is generated and tuned from 2.351 to >2.500 μm from four-wave mixing in a 0.5 cm long microwire. In a second experiment, tunable parametric sidebands are generated via modulation instability in a 10 cm long microwire. The resulting parametric frequency conversion reaches up to 49.3 THz, the largest ever reported in soft glass materials.

OCIS codes: (190.4975) Parametric processes; (190.4380) Nonlinear optics, four-wave mixing; (160.4330) Nonlinear optical materials; (160.5470) Polymers.

https://doi.org/10.1364/OL.42.000639

Mid-infrared (MIR) sources are in strong demand for medical, scientific, spectroscopic, and defense applications [1–3]. Research efforts have intensified toward the development of compact and robust MIR sources, such as fiber-based optical parametric oscillators (OPOs), all-fiber supercontinuum sources, and optical wavelength converters [4–6]. Most fiber lasers developed up to date rely on rare-earth-doped silica fibers and operate at wavelengths up to ∼2 μm, limited by the transparency window of fused silica [7,8]. Rare-earth fiber lasers compatible at longer wavelengths toward the MIR emerge gradually, including erbium-doped ZBLAN sources with emission in the range of wavelengths of 2.80, 2.94, and 3.44 μm [9–11]. It is expected that the combination of such sources with an appropriate nonlinear medium would result into broadly tunable sources, in analogy to what is performed with state-of-the-art solid-state lasers.

Chalcogenide (ChG) glasses are well known to provide transparency at wavelengths up to 12 μm and a high nonlinearity (n_2) up to 2.4×10^{-17} m^2/W [12,13]. The zero dispersion wavelengths of bulk ChG glasses (As_2Se_3 and As_2S_3) are in the MIR, i.e., ∼7 μm for As_2Se_3 and ∼5 μm for As_2S_3. Chromatic dispersion can, however, be engineered in ChG waveguides in order to shift the zero-dispersion wavelength toward shorter wavelengths and take advantage of nonlinear effects [14–17]. Using ChG microwires, the zero-dispersion wavelength has been shifted at wavelengths for which compact pump laser sources (e.g., semiconductor lasers and rare-earth-doped fiber lasers) are available, thereby providing an easy access to nonlinear parametric processes, such as supercontinuum generations [5,18], wavelength conversions [18–20], and OPOs [4,21]. Further in the MIR, a 14 cm long As_2Se_3-polymethyl methacrylate (PMMA) microwire pumped by a 10 W solid-state OPO at a wavelength of 2.6 μm generated modulation instability (MI) with frequency detuning of 30 THz (Stokes at 3.5 μm and anti-Stokes at 2.0 μm) [22]. A number of other materials have also been used to demonstrate normal dispersion four-wave mixing (FWM) or MI with frequency detuning up to ∼10 THz [23–25]. However, there is potential for greatly improving the technical specifications of all-fiber MIR wavelength converters in terms of frequency detuning, tunability, and conversion efficiency.

In this Letter, we demonstrate all-fiber and far-detuned MIR wavelength conversion from As_2Se_3 microwires. Two experiments are presented to highlight the great potential of ChG microwires for the fabrication of MIR sources. Both experiments make use of a mode-locked fiber laser centered at a wavelength of 1.939 μm. In a first experiment, an idler is generated and tuned from 2.351 to >2.500 μm resulting from wavelength tuning of a probe from 1.650 to 1.587 μm, via normal dispersion FWM in a 0.5 cm long microwire. In a second experiment, tunable sidebands up to 2.845 μm are generated via MI in the normal dispersion regime of a 10 cm long As_2Se_3 microwire. In that experiment, the frequency detuning of 49.3 THz represents the largest reported in soft glass materials.

Figure 1 shows the schematic of a microtaper. The microtaper is subdivided into a microwire, into which nonlinear processes take place, a transition section where the profile of the propagating mode is converted adiabatically, and a hybrid fiber section designed to enable efficient coupling from/to a typical low numerical aperture fiber such as SMF-28. The 0.5 cm long microwire is made out of an As_2Se_3 core, a cyclic

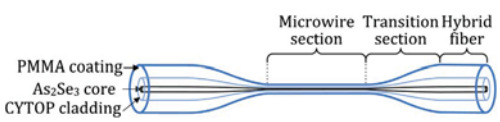

Fig. 1. Schematic of the As_2Se_3-CYTOP microtaper.

transparent optical polymer (CYTOP) cladding and a PMMA coating [18], and fabricated using the method described in [15]. The fluorine-based CYTOP polymer is transparent to wavelengths up to >2.5 μm [18]. The low refractive index of the CYTOP (1.33 at 1.939 μm [26]) makes a large refractive index contrast with respect to As_2Se_3 (2.81 at 1.939 μm [12]), thus strongly confining the propagating mode inside the microwire and enabling a large nonlinear coefficient. For a microwire core dimension in the order of the wavelength, the large refractive index contrast is also responsible for the dominant term of chromatic dispersion, namely, waveguide dispersion. For this reason, the CYTOP-cladded microwire can be set to anomalous, normal, or zero dispersion in the 1–7 μm wavelength range by an appropriate choice of the core diameter.

The FWM evolution of a picosecond pump and generated idler can be modeled by solving coupled-wave equations provided by the nonlinear Schrödinger equation. This calculation neglects pulse broadening and pulse temporal walk-off due to group velocity dispersion (GVD) [27,28]

$$\frac{dA_p}{dz} = j[\gamma_p|A_p|^2A_p + 2(\gamma_{ps}|A_s|^2 + \gamma_{pi}|A_i|^2)A_p] + 2\gamma_{pspi}A_p^*A_sA_ie^{j\Delta kz} - \alpha_pA_p/2, \quad (1)$$

$$\frac{dA_s}{dz} = j[\gamma_s|A_s|^2A_s + 2(\gamma_{sp}|A_p|^2 + \gamma_{si}|A_i|^2)A_s] + \gamma_{spip}A_pA_pA_i^*e^{-j\Delta kz} - \alpha_sA_s/2, \quad (2)$$

$$\frac{dA_i}{dz} = j[\gamma_i|A_i|^2A_i + 2(\gamma_{ip}|A_p|^2 + \gamma_{is}|A_s|^2)A_i] + \gamma_{ipsp}A_pA_pA_s^*e^{-j\Delta kz} - \alpha_iA_i/2, \quad (3)$$

where subscripts p, s, and i represent pump, signal, and idler, respectively. A_p, A_s, and A_i are electric field amplitudes. α_p, α_s, and α_i are linear attenuation coefficients. $\gamma_u (u = p, s, i)$, γ_{uv} (u, v = p, s, i and $u \neq v$), and γ_{uvkl} are the waveguide nonlinearity parameters for the self-phase modulation effect, cross-phase modulation effect, and FWM effect, respectively. Δk is the linear phase mismatch given by [27]

$$\Delta k = \frac{n(\omega_i)\omega_i + n(\omega_s)\omega_s - 2n(\omega_p)\omega_p}{c} = 2\sum_{m=1}^{\infty}\frac{\beta_{2m}}{(2m)!}\Delta\omega^{2m}, \quad (4)$$

where ω_i, ω_s, and ω_p are the angular frequencies of the idler, signal, and pump waves, respectively; $n(\omega_i)$, $n(\omega_s)$, and $n(\omega_p)$ are the effective refractive indices at ω_i, ω_s, and ω_p, respectively; β_{2m} is the $(2m)$th order dispersion coefficients; $\Delta\omega$ is the frequency difference between the pump and signal waves; and c is the velocity of light in vacuum.

To generate FWM parametric gain over a wide conversion bandwidth, the phase-matching condition must be satisfied. The effective phase mismatch is given by [27]

$$\kappa = 2\gamma P_0 + \Delta k, \quad (5)$$

where $2\gamma P_0$ is the nonlinear phase mismatch, induced by the Kerr effect, where γ and P_0 are the waveguide nonlinearity parameter and peak pump power, respectively; Δk is the linear phase mismatch given in Eq. (4). The achievement of a broad conversion bandwidth requires a far-detuned phase mismatch that is low or zero. It would thus be an asset that the nonlinear medium that serves for this wavelength conversion also has an engineerable dispersion characteristics. ChG microwires have a dispersion level that can be adjusted from an appropriate choice of geometry. Figures 2(a) and 2(b) show second-order chromatic dispersion β_2 and fourth-order chromatic dispersion β_4, respectively, as a function of core diameter of As_2Se_3 microwire and wavelength. Figure 2(c) shows the phase-matched parametric wavelengths as a function of microwire core diameter for three different pump powers, all centered at a wavelength of 1.939 μm. The phase-matched parametric wavelengths are evaluated from solving Eq. (5) while setting $\kappa = 0$. When the pump wavelength is set into anomalous dispersion, parametric wavelengths remain relatively close to the pump wavelength and depend mostly on the group velocity dispersion β_2. However, pumping in normal dispersion leads to parametric wavelengths that are widely spaced from the pump wavelength and depend strongly on the higher-order dispersion values. In both cases, as the pump power is increased, the nonlinear phase mismatch increases. As a result, the phase-matched parametric wavelengths shift further away from the pump wavelength as described in Eq. (5) and shown in Fig. 2(c).

The microtaper design selected for both experiments explained next includes a 2 cm long input/output hybrid fiber section (multimode at $\lambda = 1.939$ μm) with an As_2Se_3 core diameter of 17.1 μm, a CYTOP cladding diameter of 71.3 μm, and a PMMA coating diameter of 510 μm, a 2.3 cm long input/output transition section, and a microwire section with a core of As_2Se_3 with a diameter $\phi = 1.625$ μm, and a refractive index $n = 2.81$ at 1.939 μm [12], and a CYTOP cladding with a refractive index $n = 1.33$ at 1.939 μm [26]. This large refractive index contrast between As_2Se_3 and CYTOP leads to positive $\beta_2(\beta_2 = 3.029 \times 10^{-2}\ ps^2/m)$, negative $\beta_4(\beta_4 = -8.113 \times 10^{-6}\ ps^4/m)$, and $\beta_6(\beta_6 = -2.811 \times 10^{-10}\ ps^6/m)$, enabling phase matching over a large range of wavelengths as well as to enable a large waveguide nonlinear coefficient $\gamma = 19.7\ W^{-1}\,m^{-1}$ ($n_2 = 7.6 \times 10^{-18}\ m^2/W$ at 1.939 μm [17]) calculated by a full vectorial method [29].

In a first experiment, the stimulated FWM process in a 0.5 cm long ChG microwire is investigated. This length has

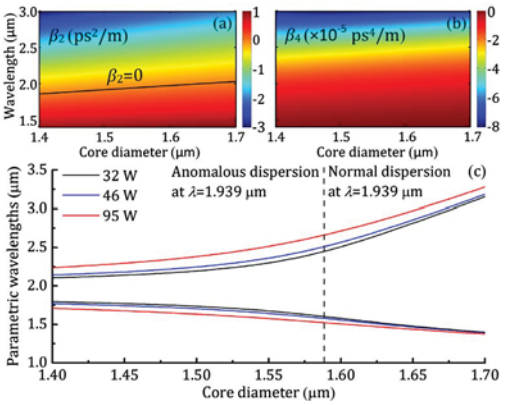

Fig. 2. (a) β_2 as a function of wavelength and As_2Se_3 microwire core diameter; (b) β_4 as a function of wavelength and As_2Se_3 microwire core diameter; and (c) phase-matched parametric wavelengths as a function of As_2Se_3 microwire core diameter. The pump wavelength is set at 1.939 μm and the peak pump power is set at 32, 46, and 95 W. The dotted line indicates the zero dispersion diameter at the pump wavelength. The microwire design includes a CYTOP cladding.

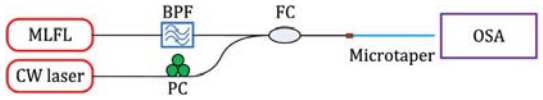

Fig. 3. Schematic of the pump–probe FWM setup. MLFL, mode-locked fiber laser; BPF, bandpass filter; FC, fiber coupler; PC, polarization controller; OSA, optical spectrum analyzer.

been chosen because it ensures that the microwire section has a constant diameter, without significant random fluctuations. Figure 3 schematizes the setup used for the pump–probe experiment. Pump pulses with a duration of 800 fs from a mode-locked fiber laser and centered at a wavelength of 1.939 μm are launched into the microwire at a repetition rate of 30 MHz. The pulses are previously broadened up to a duration of ~3.5 ps after passing through a bandpass filter with a bandwidth of 1.9 nm to increase the walk-off length. A probe signal provided by a tunable cw laser (1.490–1.650 μm) is also coupled into the microwire via a fiber coupler. A polarization controller ensures that the polarized probe couples with the polarization state of the mode-locked fiber laser. Output spectra are recorded using an optical spectrum analyzer (OSA).

Figure 4(a) shows a series of idler spectra resulting from wavelength tuning of the probe from 1.587 to 1.650 μm with a power of 0.54 mW. The pump wavelength is centered at 1.939 μm with a peak power of 3.5 W. The idler shifts in wavelength from 2.494 to 2.351 μm under the influence of the tuning probe. The measured FWM conversion bandwidth is limited at the lower limit by the maximum wavelength of the probe and on the upper limit by the OSA's spectral range of 2.500 μm.

Figure 4(b) shows the conversion efficiency (CE), defined as the output peak idler power over the input probe power. The output peak idler power is calculated using the average output

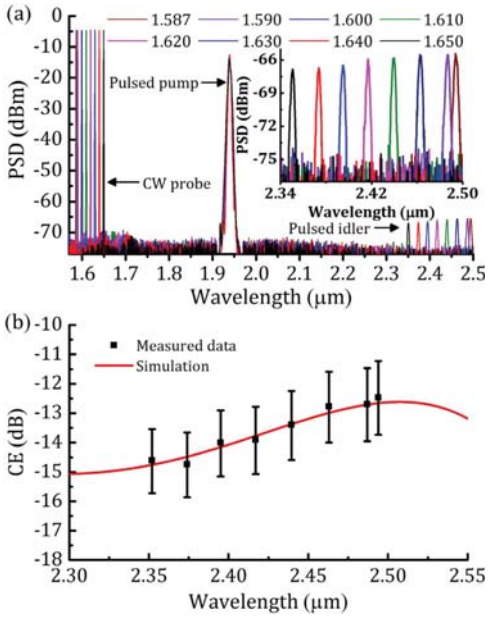

Fig. 4. (a) Measured output spectra. The legend presents corresponding probe wavelengths. The inset graph shows the zoomed-in spectra of the output idlers. (b) Conversion efficiency versus idler wavelength.

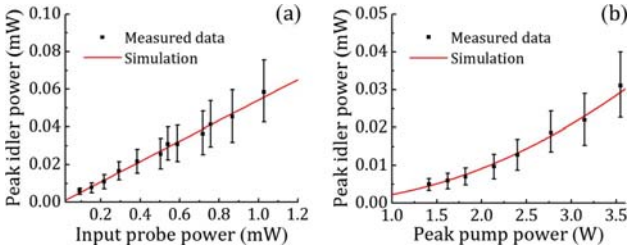

Fig. 5. (a) The output peak idler power as a function of input probe power at a fixed peak pump power $P_0 = 3.5$ W and a fixed input probe wavelength of 1.587 μm. (b) The output peak idler power as a function of peak pump power at a fixed input probe wavelength and power of 1.587 μm and 0.54 mW, respectively.

power, repetition rate, and pulse duration. The theoretical CE is evaluated from solving Eqs. (1)–(3). Those equations are valid for describing the FWM processes under the assumption of negligible pulse temporal walk-off due to GVD and pulse broadening. With 3.5 ps pump pulses in a 0.5 cm long microwire, the physical length is much shorter than the walk-off length (2.4 cm between pump wavelength of 1.939 μm and idler wavelength of 2.500 μm) and dispersion length (1.4 m at $\lambda = 1.939$ μm). Error bars take into account cumulative uncertainty on pulse duration, coupling loss, and OSA background noise.

Figure 5(a) shows the peak idler power as a function of probe power in the As_2Se_3 microwire with a fixed peak pump power of 3.5 W and a fixed input probe wavelength of 1.587 μm. The measurement is in good agreement with simulation results. Figure 5(b) shows the peak idler power as a function of peak pump power with fixed input probe wavelength and power of 1.587 μm and 0.54 mW, respectively. Again, the measurement agrees well with simulation results. The idler power can be further increased by increasing the pump power since there is no sign of saturation. Alternatively, the idler power can be further enhanced by employing a longer microwire.

In a second experiment, single pump MIR wavelength conversion via normal dispersion MI in an As_2Se_3 microwire is investigated. The microwire has a core diameter $\phi = 1.625$ μm, a propagation loss $\alpha = 0.12$ dB/cm at $\lambda = 1.939$ μm, and a length $L_w = 10$ cm. This length is chosen to preserve the walk-off length relative to the microwire length. Figure 6 schematizes the experimental setup. The mode-locked fiber laser emits pulses centered at a wavelength of 1.939 μm with a duration of 800 fs and repetition rate of 30 MHz. The laser output is launched into a 100 m long single-mode fiber to temporally broaden the pulses to 25.3 ps and increase the walk-off length (10 cm between pump wavelength of 1.939 μm and Stokes wavelength of 2.692 μm). The broadened pulses are passed through subsequent two-stage thulium-doped fiber amplifiers to enhance the output power. The amplified pulses are

Fig. 6. Experimental setup. MLFL, mode-locked fiber laser; TDFA, thulium-doped fiber amplifier; FTIR, Fourier transform infrared spectrometer.

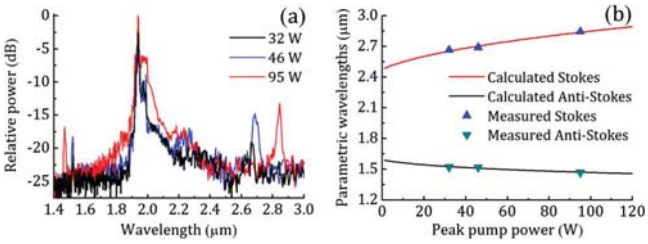

Fig. 7. (a) Measured output spectra of MI of an As_2Se_3 microwire with a core diameter of 1.625 μm and a length of 10 cm. (b) Measured and calculated parametric wavelengths as a function of peak pump power.

launched into the As_2Se_3 microwire and output spectra are recorded using a Fourier transform infrared spectrometer.

Figure 7(a) shows the output spectra of the microwire at various pump powers. The newly generated Stokes and anti-Stokes emissions are observed, widely and equally separated from the pump in the frequency domain. As the pump power launched into the microwire is increased, the anti-Stokes and Stokes bands experience a shift toward shorter and longer wavelengths, respectively. The anti-Stokes signals are generated from 1.468 to 1.521 μm, and the corresponding Stokes signals are generated from 2.845 to 2.668 μm. When the peak pump power is set to 95 W, the corresponding Stokes and anti-Stokes bands are centered at 2.845 and 1.468 μm, respectively. These two bands are symmetric in the frequency domain with a frequency shift $\Omega/2\pi = \pm 49.3$ THz. To our knowledge, this is the largest frequency shift generated by MI in soft glass materials.

Figure 7(b) shows the measured and calculated parametric wavelengths as a function of peak pump power. The experimental results are in excellent agreement with calculated parametric wavelengths from the phase-matching condition described in Eq. (5). The wavelength shift can be further increased by either increasing the pump power or tuning the pump to shorter wavelengths. The power of parametric bands can be further enhanced by either increasing the pump power or employing a longer microwire combined with longer pump pulses to preserve the walk-off length relative to the microwire length.

In summary, we have shown all-fiber parametric amplification- and MI-based MIR wavelength conversions from As_2Se_3 microwires, showing frequency conversion up to 49.3 THz. In the case of parametric amplification, the idlers are generated from 2.351 to 2.500 μm in a 0.5 cm As_2Se_3 microwire via a pump–probe scheme. In the case of MI, the widely spaced Stokes and anti-Stokes bands are generated with a frequency shift as large as 49.3 THz. The measured pump power dependence of parametric wavelengths is demonstrated and in good agreement with calculated results. The flexibility to generate parametric gain over a wide frequency range via normal dispersion parametric amplification and MI demonstrates the excellent potential of ChG microwires to provide far-detuned MIR wavelength converters and OPOs.

Funding. Collaborative Research and Development Grants Program of the Natural Sciences and Engineering Research Council of Canada (NSERC).

Acknowledgment. The authors are thankful to Coractive High-Tech for providing the chalcogenide glass used in the experiments.

REFERENCES

1. I. T. Sorokina and K. L. Vodopyanov, eds., *Solid-State Mid-Infrared Laser Sources* (Springer, 2003).
2. V. A. Serebryakov, É. V. Boĭko, N. N. Petrishchev, and A. V. Yan, J. Opt. Technol. **77**, 6 (2010).
3. U. Willer, M. Saraji, A. Khorsandi, P. Geiser, and W. Schade, Opt. Lasers Eng. **44**, 699 (2006).
4. N. Abdukerim, L. Li, and M. Rochette, Opt. Lett. **41**, 4364 (2016).
5. A. Al-Kadry, M. El Amraoui, Y. Messaddeq, and M. Rochette, Opt. Express **22**, 31131 (2014).
6. S. Xing, D. Grassani, S. Kharitonov, A. Billat, and C. S. Brès, Opt. Express **24**, 9741 (2016).
7. C. Jauregui, J. Limpert, and A. Tünnermann, Nat. Photonics **7**, 861 (2013).
8. W. Shi, Q. Fang, X. Zhu, R. A. Norwood, and N. Peyghambarian, Appl. Opt. **53**, 6554 (2014).
9. M. Bernier, V. Michaud-Belleau, S. Levasseur, V. Fortin, J. Genest, and R. Vallée, Opt. Lett. **40**, 81 (2015).
10. V. Fortin, M. Bernier, S. T. Bah, and R. Vallée, Opt. Lett. **40**, 2882 (2015).
11. V. Fortin, F. Maes, M. Bernier, S. T. Bah, M. D'Auteuil, and R. Vallée, Opt. Lett. **41**, 559 (2016).
12. Amorphous Materials, Inc., AMTIR-2: Arsenic selenide glass AsSe, http://www.amorphousmaterials.com/products/.
13. R. E. Slusher, G. Lenz, J. Hodelin, J. Sanghera, L. B. Shaw, and I. D. Aggarwal, J. Opt. Soc. Am. B **21**, 1146 (2004).
14. E. C. Mägi, L. B. Fu, H. C. Nguyen, M. R. E. Lamont, D. I. Yeom, and B. J. Eggleton, Opt. Express **15**, 10324 (2007).
15. C. Baker and M. Rochette, Opt. Mater. Express **1**, 1065 (2011).
16. C. Baker and M. Rochette, IEEE Photon. J. **4**, 960 (2012).
17. L. Li, A. Al-Kadry, N. Abdukerim, and M. Rochette, Opt. Mater. Express **6**, 912 (2016).
18. L. Li, N. Abdukerim, and M. Rochette, Opt. Express **24**, 18931 (2016).
19. R. Ahmad and M. Rochette, Opt. Express **20**, 9572 (2012).
20. R. Ahmad and M. Rochette, IEEE J. Sel. Top. Quantum Electron. **20**, 299 (2014).
21. R. Ahmad and M. Rochette, Opt. Express **20**, 10095 (2012).
22. T. Godin, Y. Combes, R. Ahmad, M. Rochette, T. Sylvestre, and J. M. Dudley, Opt. Lett. **39**, 1885 (2014).
23. P. Apiratikul, J. J. Wathen, G. A. Porkolab, B. Wang, L. He, T. E. Murphy, and C. J. K. Richardson, Opt. Express **22**, 26814 (2014).
24. L. Zhang, T. H. Tuan, H. Kawamura, K. Nagasaka, T. Suzuki, and Y. Ohishi, Appl. Phys. Express **9**, 062501 (2016).
25. C. S. Brès, S. Zlatanovic, A. O. J. Wiberg, and S. Radic, Opt. Express **19**, B621 (2011).
26. Asahi Glass Co., CYTOP, 2009, http://www.agc.com/kagaku/shinsei/cytop/en/.
27. G. P. Agrawal, *Nonlinear Fiber Optics* (Academic, 2007).
28. Q. Lin, O. J. Painter, and G. P. Agrawal, Opt. Express **15**, 16604 (2007).
29. S. Afshar and T. M. Monro, Opt. Express **17**, 2298 (2009).